Energy & Buildings 368 (2026) 117881

Contents lists available at ScienceDirect

Energy & Buildings

journal homepage: www.elsevier.com/locate/enb

# Full-year monitoring of the real-life performance of a thermochromic smart window in a tailored test building

Romy van Geijn [a,b,c], Ryan van Zandvoort [a,b], Luc Leufkens [a,b], Janique Hupperetz [a,b], David Out [a], Rémi Aninat [a], Roland Valckenborg [a], Nicole Meulendijks [a,b], Phillippe Nivelle [d,e], Michaël Daenen [d,e], Daniel Mann [a,b,c,*], Pascal Buskens [a,b,c,*]

[a] The Netherlands Organisation for Applied Scientific Research (TNO), High Tech Campus 25, Eindhoven 5656, AE, the Netherlands
[b] Brightlands Materials Center, Urmonderbaan 22, Geleen 6167, RD, the Netherlands
[c] Hasselt University (UHasselt), Institute for Materials Research (IUMAT), Design and Synthesis of Inorganic Materials (DESINe), Agoralaan Building D, Diepenbeek 3590, Belgium
[d] Faculty of Engineering Technology, Research group Engineering Materials and Applications, Hasselt University, Agoralaan Building H, Diepenbeek 3590, Belgium
[e] EnergyVille, Thor Park 8320, Genk 3600, Belgium

ARTICLE INFO

*Keywords:*
Thermochromic
Vanadium dioxide
Smart window
Solar control
Real-life performance monitoring

ABSTRACT

Thermochromic smart windows switch between transmitting and blocking solar infrared radiation (IR) based on temperature. These properties enable passive modulation of solar heat gain, which significantly lowers energy consumption in buildings and increases comfort levels for occupants via a balanced indoor climate. In this study, we set up a tailored test building in Eindhoven (The Netherlands) to monitor the real-life performance of a thermochromic smart window. We produced full sized double-glazed windows comprising a laminated outboard made from thermochromic interlayers, installed them in the test building and monitored their light transmission, solar heat gain and glass surface temperature over a full year. This enabled us to study the thermochromic phase transition of a smart window under real-life conditions for the first time. We demonstrated that the temperature of the smart window's outer glass pane regulated the phase transition and that the overall performance matched well with lab data. A glass surface temperature of 30 °C, influenced by the outdoor temperature and solar irradiance (photothermal heating), led to phase transition to the IR blocking state. During summer the smart window transitioned to its IR blocking state around 13:00, whereas in winter glass surface temperatures remained below 30 °C, retaining an IR transparent state of the smart window. In spring and autumn photothermal heating on cold, but sunny days led to undesired transitions to the IR blocking state, where glass surface temperatures exceeded outdoor temperatures by up to 20 °C. We studied the effect of photothermal heating in detail to conclude that optimized behavior of the smart window can be achieved with a phase transition temperature around 35–40 °C.

## 1. Introduction

With rising energy prices and extended heat stress in summer, building energy efficiency and new solutions for controlling a building's indoor climate become more and more important [1]. In addition to advanced insulation, novel heat pumps and on-site energy harvesting via building-integrated photovoltaics, solutions for building energy efficiency are mainly targeting windows as the element causing major heat loss in winter and solar heat gain in summer [2]. In intermediate climates optimum energy efficiency of windows can only be reached via balancing desired solar heat gain in winter with undesired solar heat gain in summer [3]. These changing requirements can only be met with adaptive solar control technologies, such as photochromic, electrochromic and thermochromic materials [4].

Thermochromic materials have shown promise as smart window technology because of the possibility to autonomously adapt a window's solar heat gain to a building's requirements based on outside temperature [5]. The intrinsic temperature-based trigger enables simple and cost-effective implementation as coating or interlayer in regular windows without special installations or adaptations. Vanadium dioxide

* Corresponding authors at: The Netherlands Organisation for Applied Scientific Research (TNO), High Tech Campus 25, Eindhoven 5656, AE, the Netherlands.
*E-mail addresses:* Daniel.Mann@TNO.nl (D. Mann), Pascal.Buskens@TNO.nl (P. Buskens).

https://doi.org/10.1016/j.enbuild.2026.117881
Received 25 March 2026; Received in revised form 2 June 2026; Accepted 29 June 2026
Available online 1 July 2026

($VO_2$) is the most prominent thermochromic material for smart window applications found in literature [6]. Its fast and highly efficient phase transition between an infrared (IR) transparent and IR blocking state at a narrow temperature, makes it a perfect candidate for highly energy efficient smart windows. In the last decades, several studies have been published investigating and optimizing different aspects of $VO_2$ for smart window applications. The thermodynamics and kinetics of the structural phase transition have been analyzed in detail [7]. Several methods to fabricate thermochromic $VO_2$ based particles [8,9], coatings [10], and nanocomposites [11] have been developed. Methods to change the phase transition temperature and optimize it for smart window applications have been investigated [7,12]. The functional performance and balance between visible transparency and solar modulation has been gradually optimized [13–15] with recent advances yielding combinations of high visible transparency around 67% with large solar modulation of 23% [16]. These advances led to researchers focusing more on the practical application of $VO_2$-based smart windows, such as investigating their theoretical maximum performance and how close current solutions are approaching these [16]. In addition, various simulation studies have been published, investigating the impact of thermochromic smart windows on a building's energy demand in different climates [17], depending on the building type [18], or depending on various material characteristics [19,20].

Even though $VO_2$-based smart window materials have been studied for a long time, real-life data on performance evaluation are lacking. So far, most studies trying to assess the performance of $VO_2$-based smart windows have focused on lab measurements combined with simulations [17–20]. Some studies have looked into building small, box-shaped test setups [21] or model houses [22,23] that were equipped with thermochromic-coated and non-coated glass plates. Via illumination with a solar or IR lamp and temperature sensors inside the boxes, or monitoring via thermal cameras and pyranometers, a comparative assessment of the cooling power of the smart window material has been executed. Some of these studies have also been using real sunlight for a more representative evaluation [24], but real performance monitoring of a smart window under normal operating conditions and real-life validation of the thermochromic phase transition have not been executed so far. These laboratory-based studies are important to gain first insights into the performance and behavior of smart window materials. However, due to various limitations, such as spectral intensity differences between artificial and natural light, or differences in heat distribution between real-sized buildings and small demos or test setups, these cannot depict the real operating conditions and therefore lead to uncertainties in relation to behavior and performance of smart windows in real buildings. Insights from real-life performance monitoring is also important to further refine simulation-based studies. It has been shown that simulation-based studies can very accurately depict real building situations [25], however the level of accuracy depends on the quality of the input data. Here more accurate performance data from real-life testing can further increase the accuracy of future simulation studies, which for smart window materials are currently solely based on lab data.

To bridge the significant knowledge gap between lab testing and real-life performance of thermochromic smart windows, which is crucial to advance the technology towards commercial application, we report a detailed investigation on the performance and functionality of a thermochromic smart window in real environment. We produced a $1 \times 1$ $m^2$ sized double-glazed smart window comprising an outboard laminated with a thermochromic polymer interlayer, installed it in a tailored test building, and monitored its functional performance for a full year. We have collected and analyzed real-life data on light and solar heat gain, connected to glass and outside temperatures to investigate the thermochromic phase transition in real-life and gain valuable knowledge to optimize performance under regular operating conditions.

## 2. Material and methods

### 2.1. Experimental procedures

#### 2.1.1. Thermochromic PVB film

Thermochromic W-doped $VO_2$ particles, with a W content of 2 at.%, were prepared using a top down approach in analogy to the method published by Calvi et al. [7,8]. Here a W-doped vanadyl oxalate precursor powder was subjected to a multi-step thermal treatment at temperatures up to 1000 °C to result in highly crystalline W-doped $VO_2$ powder. The powder material was subsequently subjected to a size reduction step via wet bead milling to obtain $VO_2$ particles with a Dx90 particle size of 87 nm (Dx50 = 32 nm, Dx10 = 15 nm), as measured by laser diffraction (Fig. S1). These particles were integrated into polyvinyl butyral (PVB) films for glass lamination in a similar manner as reported earlier [11]. Initially, a masterbatch of 1 wt% W-doped $VO_2$ in PVB was produced by dissolving PVB in ethanol and adding a dispersion of milled W-doped $VO_2$ particles in ethanol. Subsequently, the solvent was removed via evaporation and drying in a vacuum oven at 50 °C. The masterbatch was used in a compounding step, where it was mixed with virgin PVB and triethylene glycol-di(2-ethylhexanoate) (3GO), to result in a polymer composite with a $VO_2$ content of 300 ppm. The polymer composite was extruded using a 20 cm wide film die to obtain 760 µm thick films at 20 cm width.

#### 2.1.2. Fiber Bragg sensors

For temperature measurements, fiber Bragg sensors have been used, as detailed by Nivelle et al. [26]. These sensors are made of periodic structures, called fiber Bragg grating (FBG), that are inscribed in an optical fiber. The FBG locally changes the effective refractive index in the core of the fiber and therefore selectively reflects a narrow wavelength region from broad-spectrum light that is injected into the fiber. Thermal strain, expanding the fiber, will change the periodicity of the FBG and therefore changes the reflected wavelength. By calibrating the reflected wavelength against fiber temperature, the detected signal can directly be transformed into a temperature reading. Because of the spectral selectivity of the Bragg reflection, a single fiber can contain multiple gratings, enabling multiple temperature readings. Since response of an FBG can not only be influenced by temperature, but also by mechanical strain, decoupling of both effects is necessary. The decoupling of thermal and mechanical strain has been realized by the patented approach outlined by Nivelle et al., which utilizes a capillary and a lubricating liquid [26].

#### 2.1.3. Thermochromic laminate and smart window

Thermochromic laminates with integrated fiber Bragg sensors were prepared using $1055 \times 975$ $mm^2$ sized glass plates with a thickness of 4 mm. One glass plate was equipped with two fiber Bragg sensor-units using the aforementioned packaging design. To ensure a proper thermal contact while maintaining compatibility to the manufacturing process of a typical insulating glass unit (IGU), the sensor units were fixed to the glass plate using a refractive matching UV-curing adhesive. The long sensor unit (LF), containing 10 individual temperature sensing locations with a spacing of 5 cm, was placed in the middle of the glass plate directed from the center to one edge of the glass plate (Fig. S2). The short sensor unit (SF), containing 3 temperature sensors with a spacing of 5 cm, was placed at one side running towards the corner of the glass plate. The lamination stack was prepared using the glass plate with the sensor units, one layer of 760 µm thick PVB film containing thermochromic pigments, one layer of 760 µm thick pure PVB film and a second glass plate. The materials were stacked to have the sensors in the middle of the laminated stack and in direct contact with the thermochromic PVB film. Furthermore, the 20 cm wide thermochromic PVB films were placed in a manner to seamlessly flow into each other during lamination to cover the full surface area of the glass at a width of 975 mm. The lamination stack was subjected to a vacuum bed lamination process within an industrial lamination oven. Here the stack was placed in a vacuum bag and heated up to 145 °C in a multi-step lamination process with a total duration of 5 h.

The thermochromic laminated glass was integrated as outer glass pane into an IGU together with a second 4 mm thick glass plate using a 15 mm standard aluminum spacer. The gas space between the two glass plates was filled with a 93% argon atmosphere and the IGU was sealed using a standard polyurethane resin. A reference window was prepared in the same way, exchanging the thermochromic PVB film in the laminated stack with a second pure PVB film at 760 µm thickness.

#### 2.1.4. Window installation and test setup

For real-life testing, 2 smart windows and 2 reference IGUs were installed at the SolarBEAT test facilities in Eindhoven, NL. The test lab is located on the second floor of a large commercial building with the window installation in a westwards oriented façade. In addition to the fiber Bragg sensor units embedded into the smart window and reference laminate, optical sensors for detection of visible and near-infrared (NIR) light were mounted behind the center of one smart window and one reference IGU. Furthermore, a weather sensor has been placed on the roof of the test building, close to the installed windows, to monitor the external air temperature. To determine the total solar irradiance, pyranometers were placed on the outside wall next to the windows as well as within the test room, behind both the smart window and the reference IGU. All test parameters have been monitored for a full year, 24 h a day and 7 days per week.

### 2.2. Characterization methods

#### 2.2.1. UV–vis-NIR spectrophotometry

Transmission and reflection measurements of the laminated glass plates were carried out using a Perkin Elmer Lambda 750 with integrating sphere and a customized module comprising a heating/cooling element for measuring transmission and reflection in the wavelength region between 300 nm and 2400 nm at temperatures between 0 °C and 120 °C. This customized module was purchased from OMT Solutions BV. For the determination of the switching temperature ($T_{switch}$), the relative transmission at 1600 nm is plotted as function of temperature during heating and cooling, yielding a hysteresis plot. A Boltzmann fit is subjected to the heating and cooling part of the hysteresis plot and the first derivative is calculated and plotted against the temperature. $T_{switch}$ is defined as the temperature at the minimum of the derivative plot. The hysteresis width is defined as the difference between $T_{switch}$ upon heating and cooling. The hysteresis gradient is defined as the full width at half maximum of the bell shaped curve of the first derivate plot. The thermodynamic switching temperature ($T_0$) is defined as the start of the structural phase transition and was chosen as the temperature at 5% change in relative transmission.

To evaluate the optical properties of the laminated film, the luminous transmittance ($T_{lum}$, 380–780 nm) and solar transmittance ($T_{sol}$, 300–2500 nm) were calculated from the transmission spectrum according to the following equations:

$$T_{lum} = \int_{380}^{780} v_m(\lambda)T(\lambda)d\lambda \Big/ \int_{380}^{780} v_m(\lambda)d\lambda \quad (1)$$

$$T_{sol} = \int_{300}^{2500} \Phi_{sol}(\lambda)T(\lambda)d\lambda \Big/ \int_{300}^{2500} \Phi_{sol}(\lambda)d\lambda \quad (2)$$

Where $v_m(\lambda)$ is the standard luminous efficiency function for the photopic vision of the human eye, $\Phi_{sol}(\lambda)$ is the solar irradiance spectrum for air mass 1.5 (corresponds to the sun standing 37 degrees above the horizon) and $T(\lambda)$ represents the transmission of light through the laminated film at a certain wavelength (λ). Furthermore, the solar modulation efficiency $\Delta T_{sol}$ is calculated using the following equation:

$$\Delta T_{sol} = T_{sol\ (VO_2(M))} - T_{sol\ (VO_2(R))} \quad (3)$$

Transmission measurements in the real-life setup were conducted using two Ocean Optics fiber spectrometers for visible (Flame-S-VIS-NIR; range: 350–1000 nm) and NIR (NIRQuest+1.7; range: 900–1650 nm) radiation. The fiber sensors were combined in one optical cable pointing towards the center of an IGU and equipped with a collimating lens to capture light in a 180° angle. Solar irradiance was used as light source for the optical measurements. Since absolute light intensities measured by the sensors depend not only on the transparency of the window, but also on the absolute solar irradiance, sensors were placed also behind the reference window to obtain a baseline transmission, which was used to interpret the relative transmission through the smart window IGU at different daytimes, days, months and seasons.

#### 2.2.2. In-situ temperature measurements

All fiber Bragg sensor units have been calibrated prior to integration in the laminated glass stack. For calibration the glass plate with sensors was placed into a climate chamber set to a constant temperature. A fixed temperature profile was programmed into the climate chamber with an initial heating cycle from 20 to 100 °C within 4 steps, followed by a cooling cycle from 100 to −40 °C within 7 steps and a final heating cycle from −40 to 20 °C in 3 steps (Fig. S3). At each individual temperature step a 1 h isothermal was programmed. For each grating within the fibers, measurement signals were collected during the whole climate chamber cycle and calibration curves were calculated for each grating using the respective output signal and the corresponding climate chamber temperature. In the real-life setup, the fiber Bragg sensors were connected to an interrogator using a custom-built optical junction box and fiber optic cables. For each individual sensing point, measurement signals were recorded during the full year testing period at a frequency of 1 $min^{-1}$. The output signal was transformed into temperature using the calibration curves and average temperatures were calculated for the smart window and reference IGU, respectively, using datapoints from all gratings within either the LF and/or the SF.

#### 2.2.3. Outside conditions monitoring

Outside air temperature was measured using an WS600-UMB Smart Weather Sensor (Lufft, Fellbach, Germany) placed on the roof of the test building close to the installed windows. Datapoints were collected over the full year testing period at a frequency of 1 $min^{-1}$.

Solar irradiance was measured using an MS-80 Spectroradiometer (EKO Instruments, Den Haag, NL) that was placed on the outside façade next to the test windows. Additional spectroradiometers were placed within the test room behind each the smart window and the reference IGU. Datapoints were collected over the full year testing period at a frequency of 1 $min^{-1}$.

## 3. Results and discussion

### 3.1. Window preparation and installation of test setup

Thermochromic PVB films were prepared by integrating highly crystalline W-doped $VO_2$ (M) nanoparticles with an average particle size <100 nm into PVB via liquid dispersion and solvent evaporation to create a solid masterbatch with a particle content of 1 wt%. The final concentration of 300 ppm functional material was adjusted by compounding the masterbatch with an appropriate amount of virgin PVB and 20 wt% of plasticizing agent. The composite material was extruded using a film die to produce several meters of 20 cm wide film with an average thickness of 760 µm. For lab scale validation, the film was used to laminate two 10 × 10 $cm^2$ glass plates via a hot press. Analyzing the light transmission of the thermochromic laminate via UV–vis-NIR spectrophotometry at 0 °C, resulted in $T_{sol}$ and $T_{lum}$ values of 62.5% and 64.6%, respectively (Fig. 1a). Performing the same measurement at elevated temperatures resulted in increased absorption in the IR region, because of the phase transition from $VO_2$ (M) to $VO_2$ (R). Therefore, the $T_{sol}$ was reduced to 56.6%, resulting in a $\Delta T_{sol}$ of 5.9%. Even tough the

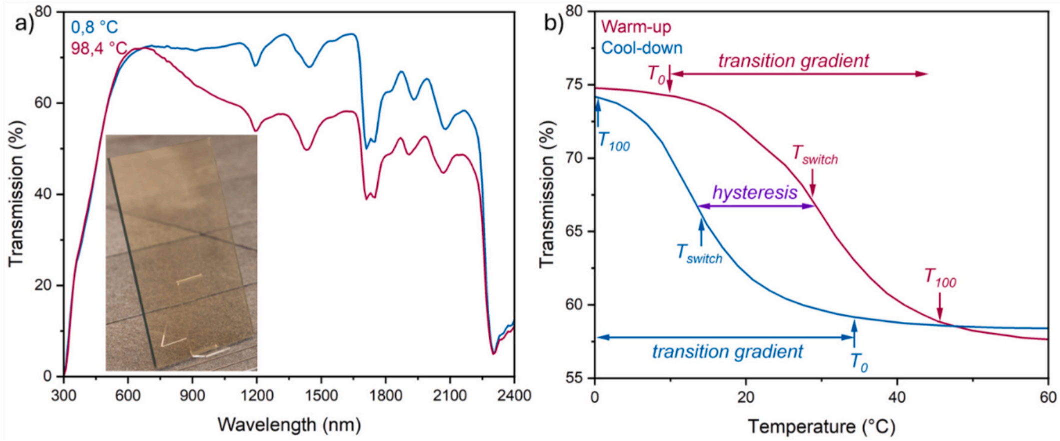


**Fig. 1.** a) UV–vis-NIR transmission spectra of the thermochromic laminate measured in the cold (blue line) and hot (red line) state (note: absorption bands >1200 nm present in both cold and hot transmission spectrum are caused by the PVB interlayer); inlay showing a picture of a thermochromic laminate. b) Hysteresis measurement of the temperature dependent transmission at 1600 nm wavelength of a thermochromic laminate during heat up (red) and cool down (blue); phase transition characteristics, such as $T_0$, $T_{switch}$, transition gradient and hysteresis, are indicated. (For interpretation of the references to colour in this figure legend, the reader is referred to the web version of this article.)

balance of $T_{lum}$ and $\Delta T_{sol}$ obtained is not best in class for thermochromic coatings and films reported in literature, it is well in line with average reported material properties and therefore well suited to generate insights into real life behavior of thermochromic smart windows. To analyze the switching temperature and hysteresis of the thermochromic laminate, we performed a hysteresis measurement, recording the temperature dependent transmission at 1600 nm wavelength (Fig. 1b). We observed a $T_{switch}$ from monoclinic to rutile at 29.7 °C, a $T_0$ at 12.7 °C and a transition gradient of 34.9 °C. For the transition from rutile to monoclinic we observed a $T_{switch}$ at 13.9 °C, a $T_0$ at 36.4 °C and a transition gradient of 35.6 °C, resulting in a hysteresis width of 15.8 °C.

To produce the thermochromic smart window, the thermochromic PVB films were used in a vacuum bed lamination process to connect two 4 mm thick glass plates at a size of 1055 × 975 mm$^2$. Fiber Bragg sensors were integrated into the lamination stack to enable temperature measurements within the thermochromic laminate. The as prepared thermochromic laminates were integrated as outer glass pane into an IGU together with another 4 mm thick glass plate and a 15 mm aluminum spacer. The gas space was filled with argon and sealed using a polyurethane resin. The resulting smart window IGUs had a visible transmission $T_{lum}$ of 59%, a cold state g-value (or shgc) of 60%, a hot state g-value of 56% and a U-value of 2.62 W/m$^2$K. Here it has to be noted that the U-value was not optimized to fulfil current building regulations in the Netherlands, which ask for U-values of <1.2 W/m$^2$K. However, since thermal insulation was not part of this study, the windows U-value does not impact this investigation and was therefore neglected. For real-life performance monitoring, two thermochromic IGUs, as well as two reference IGUs, were installed at the SolarBEAT test facilities in a second story, westwards facing façade, in Eindhoven (Fig. 2). The fiber Bragg sensors were connected to an interrogator via an optical junction box and fiber optics cables, and a spectrophotometer for monitoring UV and NIR radiation was mounted behind a thermochromic smart window IGU, as well as behind a reference IGU.

### 3.2. Performance validation

To validate the performance of the thermochromic smart window in real-life, we compared the IR transmission between lab measurements and measurements from the test facilities. For this comparison, we calculated expected transmission spectra using lab measurements from the individual components of the smart window and reference IGU and the AM1.5 solar spectrum (Fig. 3a). For the smart window in the cold state we used a transmission spectrum of the thermochromic laminate at 0 °C, a spectrum of 4 mm ultra clear glass and solar AM1.5. For the smart window in the hot state, we used the same components, but exchanging the thermochromic laminate transmission data for a spectrum recorded at elevated temperatures. Since the real-life measurement uses natural sunlight as light source, the measurement through a reference IGU is


**Fig. 2.** Window installation at the SolarBEAT test site. a) Westward facing façade with the 2 installed smart windows (green square) and the 2 installed reference IGUs (blue square). b) Look through one of the smart windows from inside out with pyranometer installed at the middle of the window. (For interpretation of the references to colour in this figure legend, the reader is referred to the web version of this article.)

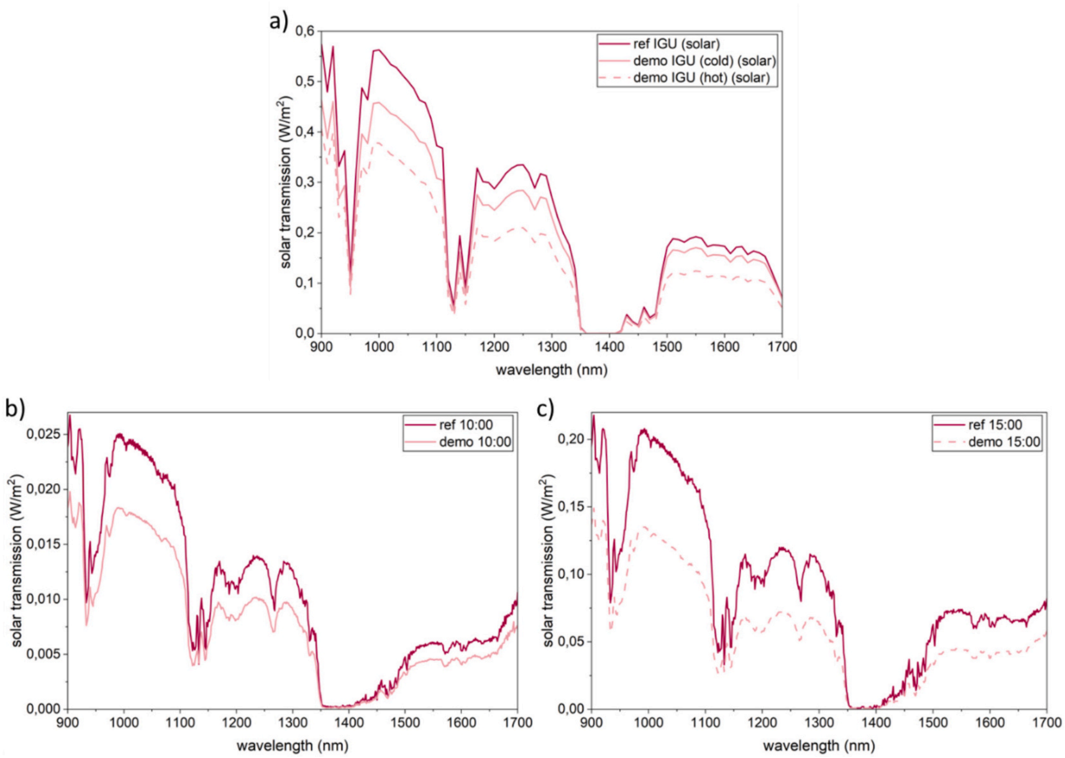


**Fig. 3.** a) Expected transmission spectrum of reference window (magenta) and smart window in the cold (light pink, full) and hot (light pink, dotted) state; and measured transmission spectra of reference window (magenta) and smart window (light pink) in real environment at b) 10:00 and c) 15:00 on May 10th 2022. (For interpretation of the references to colour in this figure legend, the reader is referred to the web version of this article.)

needed to account for the varying intensity of the light source. Therefore, we also calculated an expected transmission spectrum for the reference IGU. Here we used transmission data from a laminate made from two 4 mm thick glass plates and commercial PVB as interlayer, a spectrum of 4 mm ultra clear glass and solar AM1.5. For validation of the real-life data, we measured the NIR transmission through the smart window and reference IGU on May 10th 2022. The day was selected since it was expected that the cold temperatures in the morning would enable a measurement comparable to the cold state measurement in the lab, and that rising temperatures in the afternoon would lead to a phase transition, yielding transmission data that are comparable to the hot state measurement from the lab. The first measurement was performed at 10:00 am at an outside temperature of 8 °C (Fig. 3b). The temperatures measured within the thermochromic laminate and the reference laminate were slightly higher at 9.7 and 8.7 °C, respectively. According to the $T_0$ measurements from the lab, the functional $VO_2$ material should be in the monoclinic crystal phase at this temperature. Comparing the transmission data from the real-life measurement with the expected spectrum calculated from lab data in a wavelength region between 900 and 1700 nm, an overall good match in relative transmission up to 1600 nm can be observed. Above 1600 nm the transmission spectrum from the real-life experiments starts to deviate, which can be correlated to the lower accuracy of the spectrophotometer in these wavelength regions. For a more detailed comparison of the relative transmission through the thermochromic smart window, the transmission ratio between the smart window and reference IGU at a single wavelength was calculated and compared to the expected ratio from lab measurements of the cold state smart window and reference IGU. The wavelength that was selected for this comparison was 1000 nm, since a relatively high solar intensity is present at this wavelength and a significant transmission difference between smart window and reference IGU is expected, which reduces the impact of noise from the real-life setup. From the lab measurements a transmission ratio at 1000 nm between the cold state smart window and the reference IGU of 0.80 was expected. The real-life measurement resulted in a ratio of 0.75. The slightly lower transmission ratio can either mean that a small part of the functional $VO_2$ (M) is already transitioned to the $VO_2$ (R) state, or it can be attributed to inaccuracies because of the low light intensity in real life, which comes close to the detection limit of the spectrophotometer and therefore leads to a larger error margin.

The second measurement was performed at 15:00 on the same day at an outside temperature of 16 °C (Fig. 3c). Because of the intense solar irradiation of 533 W·m$^{-2}$ on the west façade, the glass of both windows showed a significantly higher temperature. Within the reference IGU a temperature of 26 °C was measured, which shows that light absorption of regular glass leads to a temperature increase of 10 °C in the laminate in comparison to the outside air temperature (photothermal heating). For the thermochromic laminate an even higher temperature of 32 °C was measured, representing a further temperature increase of 6 °C due to the absorption of the functional material in the laminate. The hysteresis measurements from the lab suggest that at 32 °C approximately 60% of the $VO_2$ (M) is transitioned to $VO_2$ (R). Comparing the transmission data from the real-life measurement with the expected spectrum calculated from lab data, again an overall good match in wavelength regions between 900 and 1600 nm can be observed. For a more detailed analysis we also calculated the transmission ratio at 1000 nm between the reference and the smart window IGU and compared the obtained value to the ratio from the expected spectra for the reference IGU and the smart window IGU in the hot state. For the real-life data a ratio of 0.66 was obtained, which is very close to the expected ratio of 0.68. Combining the cold and hot state measurements for the smart window, a change in transmission ratio of 12% upon transition from cold to hot was expected from the lab measurements, whereas in the real-life measurement a change of 9% was observed. The main difference between expected and measured results comes from a lower than expected transmission ratio in the cold state. With these results we can verify that a phase transition from transparent to blocking state of the smart window has occurred in the real-life experiment and that the extent of the transmission modulation was in good agreement with the expected effect. Therefore, a qualitative and quantitative validation of the thermochromic performance of the smart window was achieved.

### 3.3. Full-year performance monitoring

After validating the performance of the smart window in real-life, we continued the outdoor measurements over a full year. All mentioned data were gathered continuously in a period between April 2022 – March 2023.

#### 3.3.1. Daily data analysis and interpretation

For the daily data analysis, 3 sets of data were collected (Table 1). First the spectral data were collected from the spectrophotometers placed behind the smart window and reference IGU. Secondly, the temperature data were collected from the fiber Bragg sensor units inside the smart window and reference IGU, as well as from the weather sensor on the roof. Thirdly, the solar irradiance data were collected via the pyranometer on the outside façade.

*3.3.1.1. Spectral data analysis.* For analysis of the spectral data, the transmission levels at 1000 nm through the smart window and reference IGU were plotted against the time of day. Since transmission levels are wavelength and time dependent, a single wavelength was chosen for analysis for simplification. It was shown in chapter 3.2 that at 1000 nm a significant difference between reference and smart window IGU is present, as well as a well detectable change in transmission through the smart window upon switch from the cold to the hot state. Therefore, the transmission at 1000 nm is a good measure to investigate the thermochromic switch in the real-life situation. Since the transmission through both windows was constantly changing during the day, because of the movement of the sun, the transmission ratio between the reference and smart window IGU was calculated to detect the thermochromic switch in transmission.

On a fully sunny day a well-defined trend in transmission over the full daytime can be observed (Fig. 4a). From morning until noon the west façade, where the windows are implemented, sees only diffuse sunlight, which leads to very low transmission levels through both windows between 0.01 and 0.04 $W \cdot m^{-2}$ at a wavelength of 1000 nm. Initially, from 6:30 in the morning, when the measurement starts, until around 9:30 a small but steady increase in transmission can be observed, before a plateau value is reached between 9:30 and 13:00. Both transmission through reference and smart window IGU show the same trend during this time of day, with the smart window showing slightly lower transmission levels than the reference window. From approximately 13:00 onwards direct sunlight starts hitting the west façade, which leads to a sharp increase in transmission through both windows until a maximum transmission is reached around 18:00. Using a solar tracker, we could show that at this time of day, the sun is facing the west façade in almost a 90° angle, which explains the highest measured irradiance. After 18:00 the transmission starts to drop until 19:30, where a significant drop in transmission is observed in both windows, caused by shading from an adjacent building. Afterwards, the transmission slowly drops to 0 until sunset. During the time of direct sunlight the transmission through the reference window increases much more rapidly than through the smart window, leading to an increased transmission gap between both windows. The reference window reaches maximum transmission values at 1000 nm wavelength of 0.38 $W \cdot m^{-2}$ at 18:00, whereas the smart window only reaches a maximum of 0.25 $W \cdot m^{-2}$. This increased difference, is already a first indication of the thermochromic switch towards reduced transmission in the hot state.

To analyze the relative transmission through the smart window in more detail, the transmission ratio between the smart window and reference IGU was calculated and plotted in the same graph (Fig. 4a). Here a relatively steady ratio around 0.74 is obtained in the morning between 9:30 and 13:00. At 13:00, when direct sunlight starts hitting the west façade, an immediate drop in transmission ratio to 0.55 is observed, followed by a slow but steady increase in ratio until 18:00, where a plateau value of 0.66 is reached. This behavior can be attributed to the changing angle of incidence from sunlight on the façade. At 13:00, sunlight starts hitting the facade at a very small angle, which leads to a significantly longer pathway of light through the functional interlayer of the smart window and therefore to more absorption. With progressing time and movement of the sun, the sunlight angle of incidence increases until it reaches approximately 90° at 18:00. This coincides with a reduced pathway of light through the functional layer and therefore an increased transmission ratio. The thermochromic switch in transmission adds further complexity to the interpretation of the transmission ratio in the time period between 13:00 and 18:00. Since the phase transition from $VO_2$ (M) to $VO_2$ (R) reduces the light transmission at 1000 nm, balancing effects can be observed in the transmission ratio. That a thermochromic switch occurs in the smart window can be concluded from the fact, that the transmission ratio does not reach the same value as before 13:00, and that the 18:00 transmission ratio is in good agreement with the expected ratio from lab measurements.

To confirm the angle dependent effect on the transmission ratio, we analyzed the time dependent transmission trough both windows at 500 nm, where no change in transmission occurs upon phase transition from $VO_2$ (M) to $VO_2$ (R). Here the same drop in transmission ratio at 13:00 is observed as for the transmission at 1000 nm, with a subsequent ratio increase until 18:00. However, for the transmission at 500 nm, the ratio between reference and smart window reverts back to the initial value, so that at the plateau between 9:30 and13:00 and at 18:00 the same transmission ratio of 0.60 is obtained (Fig. S4).

**Table 1**
Key data collected for 4 representative days which are analyzed in Section 3.3.1.

| | | Sunny day (August 13th 2022) | Cloudy day (August 15th 2022) | Day starting sunny and ending cloudy (October 6th 2022) | Day starting cloudy and ending sunny (June 4th 2022) |
|---|---|---|---|---|---|
| Maximum transmission at 1000 nm [$W/m^2$] | Reference window | 0.38 | 0.17 | 0.33 | 0.41 |
| | Smart window | 0.25 | 0.10 | 0.22 | 0.27 |
| Morning transmission ratio | | 0.74 | n.a. | 0.74 | n.a. |
| Transmission ratio at 13:00 | | 0.55 | n.a. | 0.55 | 0.56 |
| Transmission ratio at 18:00 | | 0.66 | n.a. | n.a. | 0.66 |
| Maximum temperature [°C] | Ambient | 31.4 | 25.5 | 17.9 | 25.2 |
| | Reference window | 45.3 | 29.6 | 27.5 | 40.5 |
| | Smart window | 55.8 | 33.4 | 36.8 | 50.8 |
| Minimum temperature [°C] | Ambient | 18.7 | 21.5 | 10.6 | 12.8 |
| | Reference window | 18.9 | 21.9 | 10.7 | 15.2 |
| | Smart window | 19.1 | 22.1 | 10.9 | 15.4 |
| Maximum irradiance (west façade) [$W/m^2$] | | 784 | 424 | 718 | 741 |

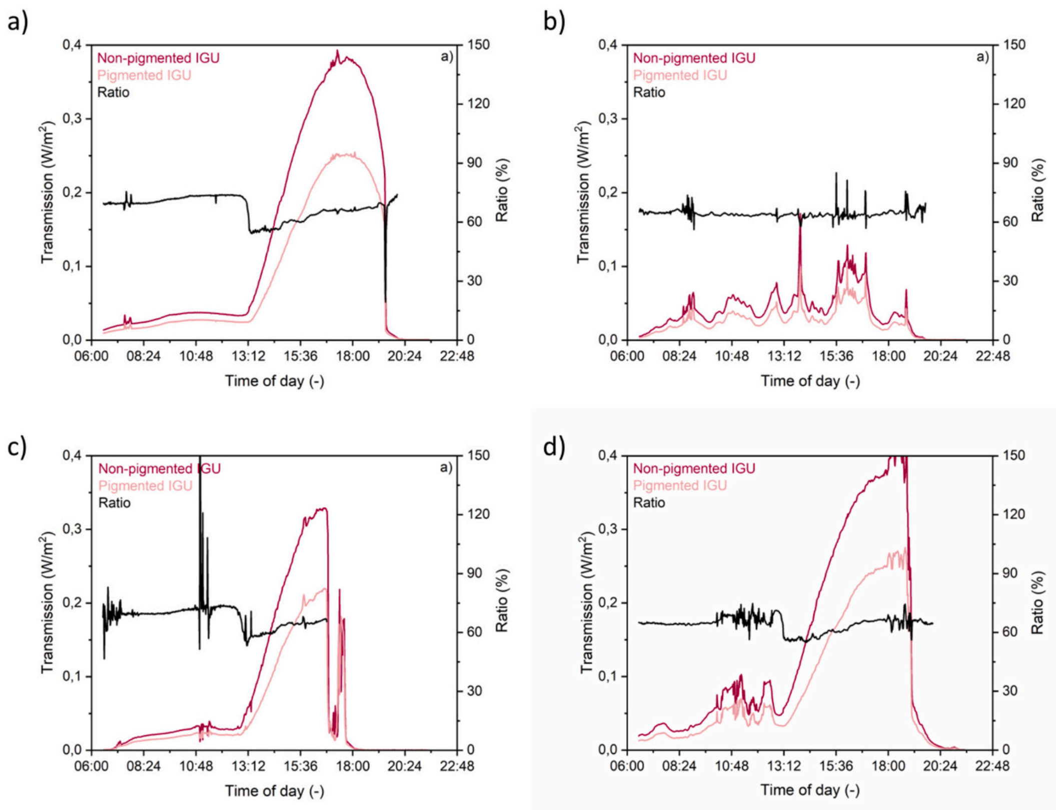


**Fig. 4.** Time dependent transmission spectra at 1000 nm of reference window (magenta) and smart window (light pink) and transmission ratio (black) for a representative a) sunny day (August 13th 2022), b) cloudy day (August 15th 2022), c) day starting sunny and ending cloudy (October 6th 2022) and d) day starting cloudy and ending sunny (June 4th 2022). (For interpretation of the references to colour in this figure legend, the reader is referred to the web version of this article.)

To detect the thermochromic switch for individual sunny days, we can therefore use the transmission ratio in the morning at diffuse sunlight, here we use the ratio around 12:00, shortly before directly sunlight hits the west façade, and compare it to the transmission ratio at 18:00 where direct sunlight is almost perpendicular to the windows. Here a significant difference between both ratios of 8–10% indicates the transition from $VO_2$ (M) to $VO_2$ (R) during the day.

For cloudy days, the measured transmission of sunlight at 1000 nm wavelength through both windows is at relatively low levels, mostly below 0.1 $W \cdot m^{-2}$, and is fluctuating a lot over the day (Fig. 4b). In general, the transmission through the reference window is slightly higher than through the smart window, however transmission spikes from diffuse light are not always happening at the same time for both windows. This can be explained by clouds that are moving and therefore both windows will not always see the same light intensity. This effect also makes the transmission ratio difficult to interpret, since a spiking pattern is obtained for moments with unequal light distribution over both windows. In general a very steady transmission ratio is obtained, which can be interpreted as a steady state in the smart window and no thermochromic switch occurring. However, since the low overall light intensity increases the error margin in the detected signal and since the uneven light distribution leads to a spiking pattern and errors in the calculated ratio, interpretation of the thermochromic switch solely based on the transmission signal is not possible. Here also the temperature measurements need to be used to correctly interpret the $VO_2$ phase transition.

For days that are partially sunny and partially cloudy, a case-by-case analysis is required to judge the thermochromic switch, dependent on the intensity of clouding and the time of day that is sunny or cloudy. Examples are days that are mostly sunny in the morning and noon, but cloudy in the afternoon (Fig. 4c), or days that are cloudy in the morning but sunny in the afternoon (Fig. 4d).

For days that are sunny in the morning, the overall behavior at that time of day is comparable to a fully sunny day and the 12:00 transmission ratio can be calculated and interpreted as shown above. When it becomes cloudy in the afternoon, which can lead to 1000 nm transmission levels dropping to $<0.1\ W \cdot m^{-2}$, the transmission ratio cannot be interpreted any more due to reasons explained for fully cloudy days. Here the last possible transmission ratio that can be calculated needs to be used for interpretation of the thermochromic switch, taking into account that the obtained ratio shows a certain error due to the angle of incidence of sunlight at the respective time of day.

For days that start cloudy, the 12:00 ratio cannot be interpreted, which complicates the interpretation of the $VO_2$ state at the beginning of the day. Here temperature data is required to judge if the smart window is in the transparent $VO_2$ (M) state or the blocking $VO_2$ (R) state at the start of the day. When the clouds disappear during the day, so that the afternoon becomes sunny, the 18:00 ratio can be calculated and interpreted as discussed above for fully sunny days. All other partially cloudy days have to be judged case-by-case together with the temperature data.

*3.3.1.2. Temperature data analysis.* For the temperature measurements, the datapoints from the fiber Bragg grating (FBG) sensor units within the reference and smart window IGU were used. For each window 2 fibers with in total 13 gratings were present. A short fiber (SF) with 3 gratings was localized at the side of the window running towards the bottom corner and a long fiber (LF) with 10 gratings was localized running from the center of the window towards the bottom edge.

First we started by analyzing the temperature signal obtained from the individual gratings at a sunny day. Within individual fibers, the measured temperatures from different gratings showed only small variations. During times of day with mainly diffuse sunlight, only a spread of <1 °C between the 10 gratings in the LF was observed, which indicates a very homogeneous glass temperature between the center and the edge (Fig. S5a). At direct sunlight, when measured glass temperatures rise above 50 °C, the spread between gratings rises up to 1.9 °C, with gratings at the edge showing in general slightly higher temperatures than grating at the center of the window. For the SF under diffuse light also only a very small spread <0.5 °C between the 3 gratings was observed, however under direct light the spread increased up to 4.7 °C (Fig. S5b). Here the grating located in the corner of the window, showed the lowest temperature, whereas the grating which was the furthest away from the corner showed the highest temperature. Comparing the temperatures measured from the LF and SF with each other, it was observed that under diffuse sunlight a good match between measurements from both fibers was obtained. However, under direct sunlight at high temperatures a significant difference between both sets of data, with the SF showing significantly lower temperatures, was observed. It can also be observed that the temperature increase for the SF under direct sunlight is not as steep as for the LF. Since the SF was located at a part of the window that was subjected to shading from the frame, the lower overall temperatures can be explained. The overall lowest temperature was measured from the grating directly in the corner of the window. Therefore, it can be concluded that the windows show a very homogeneous temperature over most of the surface area, as well under diffuse as under direct sunlight, but that at very high temperatures >50 °C, the corners can have a temperature that is up to 10% lower than the rest of the window.

For temperature analysis of individual days, we used the temperature data from the LF and calculated an average temperature from all 10 gratings. This average temperature was used to investigate the glass temperature for the reference and smart window over the full day and was compared to the ambient temperature that was measured via a weather sensor placed on the roof of the test building, close to the installed windows.

For sunny days the ambient temperature follows a slow but steady decrease from the start of the day until shortly before sunrise (Fig. 5a). At sunrise, the temperature starts to increase, before reaching a plateau value between 11:00–20:00, during which only a minor temperature rise occurs. At the end of the day, during sunset, the ambient temperature decreases again slowly, but steadily. The glass temperature for both windows follows the ambient temperature rather precisely during night and at diffuse sunlight. However, at direct sunlight the windows start to warm up much more rapidly and reach significantly higher temperatures. Here the temperature profile of both windows follow the general trend of the solar irradiance levels on the west façade (vide infra). Starting around 13:00, the glass temperature in the reference IGU rises within 5 h from 30 to 45 °C, reaching temperatures that are 50% higher than ambient, until it starts dropping again from 17:00 onwards. For the smart window this rise in temperature is even more extreme. Here the glass temperature rises between 13:00 and 17:00 from 30 to 56 °C, reaching temperatures that are almost double the ambient. At the end of the day, both windows cool down again towards the ambient temperature around 20 °C. This high temperature, which deviates significantly from ambient, is important for the performance of the smart window, since this means that the functional $VO_2$ experiences a significantly higher temperature at direct sunlight than ambient or regular glass temperatures. Here, the additional increase of 11 °C over the reference window can be attributed to light absorption of $VO_2$ in the functional interlayer.

To verify the temperature increase of the $VO_2$ containing PVB interlayer upon irradiance, we performed a lab experiment in which we exposed $VO_2$ powder to light from a solar simulator at various light intensities. While maintaining a constant temperature of 20 °C of the

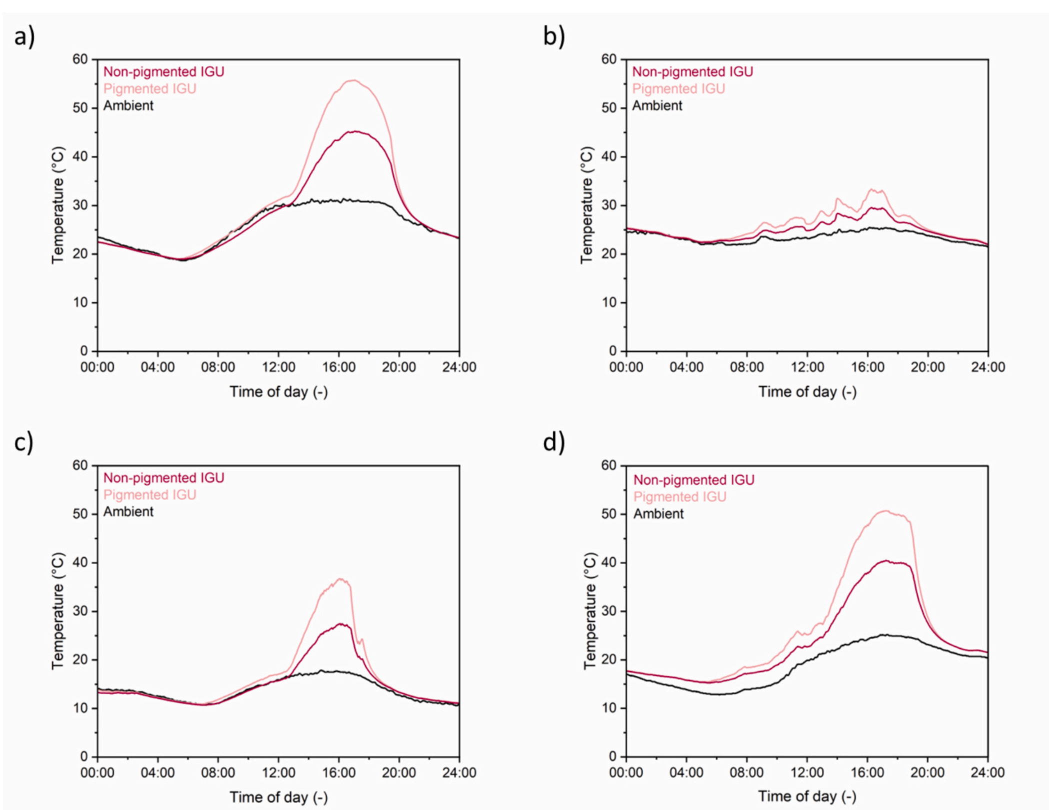


**Fig. 5.** Time dependent temperatures measured of reference window (magenta) and smart window (light pink) and ambient (black) for a representative a) sunny day (August 13th 2022), b) cloudy day (August 15th 2022), c) day starting sunny and ending cloudy (October 6th 2022) and d) day starting cloudy and ending sunny (June 4th 2022). (For interpretation of the references to colour in this figure legend, the reader is referred to the web version of this article.)

surrounding, we measured the temperature within the $VO_2$ powder using an immersed fiber Bragg sensor. Here we could show that whilst illuminating the powder for 2 min each with an intensity between 600 and 1200 $W{\cdot}m^{-2}$, the temperature in the powder increased at a constant rate of 0.012 $^{\circ}C{\cdot}m^2{\cdot}W^{-1}$, confirming the effect of photothermal heating (Fig. S6a). For further validation of the effect, we performed the same experiment at a constant external temperature of 35 °C, where exactly the same trend of temperature increase with a rate of 0.012 $^{\circ}C{\cdot}m^2{\cdot}W^{-1}$ was obtained (Fig. S6b). The temperature increase of 10 °C for illumination with 800 $W{\cdot}m^{-2}$ that was reached in the lab setup, corresponds very well with the increased temperature of 11 °C observed in the real-life setup.

For cloudy days, the general trend in ambient temperature is the same as for sunny days, but much less pronounced (Fig. 5b). A temperature decease until sunrise is followed by a slight temperature increase until sunset, followed by another slight temperature decrease. Within the period of 24 h the ambient temperature only varies between 21.5 and 25.5 °C. The glass temperatures in both windows follow the trend of the ambient temperature to a large extent over the full day. Only small temperature spikes can be observed that correspond to spikes in solar irradiance levels measured via the pyranometer (vide infra). In general, these temperature spikes are more pronounced in the smart window where a maximum temperature of 33 °C is reached, representing a 29% temperature increase in comparison to ambient, whereas the reference window only reached a maximum temperature of 29.5 °C, and a relative increase of 16%. Since the temperature data from the smart window can be used independently of data from the reference IGU, differences in temperature spikes between both windows caused by cloud movement do not interfere with data interpretation. Therefore, the temperature data from the smart window IGU, together with lab data on switching hysteresis, can be used to interpret the functional state of the thermochromic material, when spectral data cannot be analyzed because of uneven light distribution as discussed in Section 3.3.1.1.

On partial cloudy days, the ambient temperature again follows a similar general trend as on sunny days. Deviations occur when the afternoon is cloudy, which leads to an earlier temperature drop (Fig. 5c), or when the morning is cloudy, which leads to a slower temperature increase in the morning and the maximum temperature being reached at a later time of day (Fig. 5d). Furthermore, the season and the overall irradiance levels influence the average temperature and temperature range of the specific day as well as sunrise and sunset hours, which influence at which time of day temperatures rise or fall. The glass temperatures of both windows mostly follow the ambient temperature with no or only diffuse sunlight. With direct sunlight a rapid temperature increase can be observed for both windows, following the general trend of solar irradiance levels (vide infra). The glass temperature of the reference window on partial cloudy days can reach up to 60% of the respective ambient temperature, during times of direct sunlight. In the smart window, the glass temperature can be even higher, up to double the respective ambient temperature. In general. The glass temperature of both windows during times of direct sunlight show the same behavior as on sunny days, whereas during times of diffuse sunlight, the same behavior as on cloudy days can be observed.

*3.3.1.3. Solar irradiance analysis.* For analysis of solar irradiance levels on the west façade, we used the outdoor pyranometer that was located on the façade next to the test windows. For sunny days, sunrise and sunset can be very well tracked via the solar irradiance levels, as well as the difference between diffuse and direct sunlight on the west façade (Fig. 6a). For a typical sunny day in August, the irradiance levels start to rise around 5:30 and go down to 0 again at 20:00. This corresponds well with sunrise and sunset in Eindhoven, with the only significant deviation being at sunset, where measured irradiance levels are impacted by an adjacent building that leads to shading of the west façade at the end of

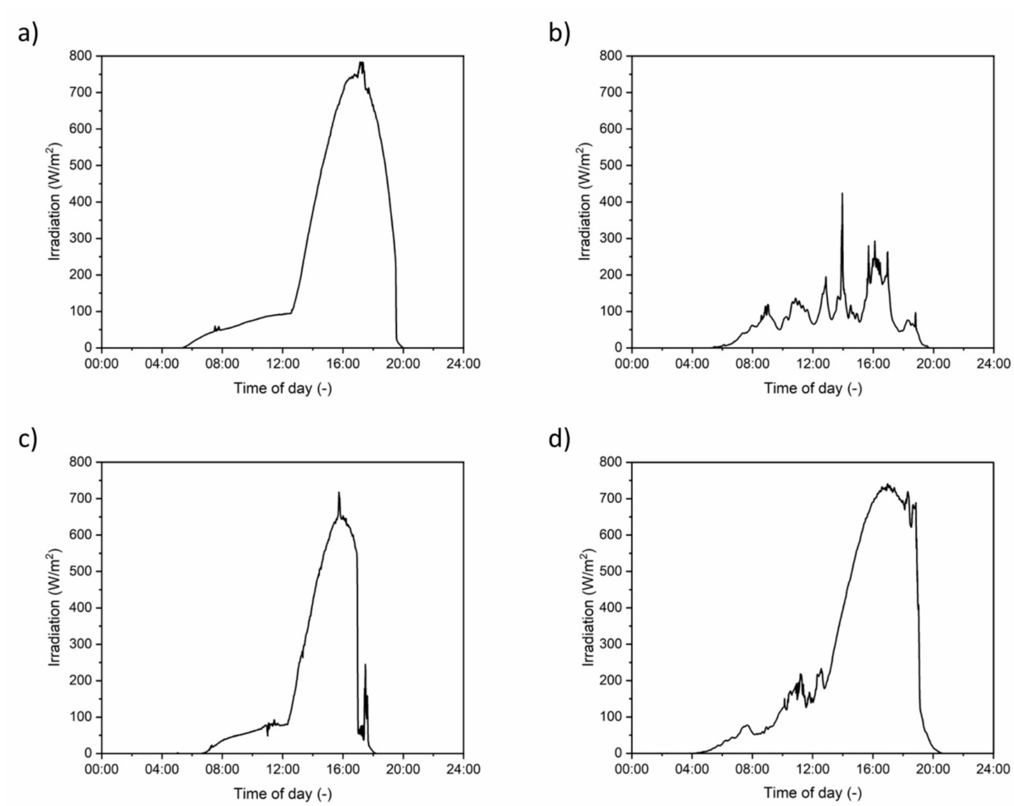


**Fig. 6.** Time dependent solar irradiance levels for a representative a) sunny day (August 13th 2022), b) cloudy day (August 15th 2022), c) day starting sunny and ending cloudy (October 6th 2022) and d) day starting cloudy and ending sunny (June 4th 2022).

the day. From 5:30 until 12:30 irradiance levels show a slow but steady increase up to 100 W·m$^{-2}$, representing times of diffuse sunlight on the west façade. With direct sunlight hitting the west façade, irradiance levels start to rise significantly to reach up to 750 W·m$^{-2}$ around 17:00, before they start to drop again until 20:00.

On cloudy days, sunrise and sunset times are not impacted. Therefore, the times where irradiance levels start to rise above 0 and drop towards 0 are similar as on sunny days. However, the overall trend during the day differs significantly (Fig. 6b). An irregular irradiance profile is observed that is governed by the movement of clouds and no clear distinction between diffuse and direct sunlight can be observed. Overall irradiance levels stay rather low <200 W·m$^{-2}$, with short irradiance spikes with more than double the intensity. These spikes are caused by light reflection from clouds or other objects that are detected by the pyranometer and can also be observed on sunny days, but with a significantly lower intensity.

For partial cloudy days, the overall irradiance profile is similar to sunny days with deviations during times of cloud movement (Fig. 6c,d). Here similar total irradiance levels as well as similar times at which irradiance levels rise and drop, or change from diffuse to direct irradiance can be observed. The main difference in these values can be related to seasonal variations in sunrise and sunset times as well as total solar irradiance levels. Cloud movement can lead to dropping irradiance levels, but also to irradiance spikes because of light reflection from clouds. This can also lead to difficulties in detecting the exact time of day where direct sunlight starts hitting the west façade.

### *3.3.2. Monthly overview*

With light transmission and temperature of the thermochromic smart window and reference IGU, as well as solar irradiance levels having been analyzed for individual days, the smart windows performance and behavior can be analyzed for full months. To analyze the state of the smart window, we use the transmission ratio at 12:00 and 18:00 for the individual days as well as the maximum and minimum temperature reached in the smart window. As discussed in Section 3.3.1.1., during sunshine we can use the transmission ratio between smart window and reference IGU to determine if the smart window is in the monoclinic or rutile state at the start of the day and during times of direct sunlight on the west façade. For cloudy days, as discussed in Section 3.3.1.2., we additionally use the maximum temperature in the smart window in combination with the lab data on the switching temperature, to determine if a phase transition to the rutile state has occurred on individual days. For all days, the minimum temperature in the smart window can be used to determine if a switch back to the monoclinic state has occurred during the night, or if the smart window stayed in the rutile state. To relate the behavior of the smart window to the outdoor environment, we additionally analyze the maximum outdoor temperature reached on individual days and put it in relation to the window temperature and state of the smart window.

Using August 2023 as representation for a regular summer month in the Netherlands, it can be seen that overall relatively high outdoor temperatures are reached (Fig. 7a). The maximum temperature reached for induvial days in that month was between 21.1 and 33.3 °C. The maximum temperature reached in the smart window is significantly higher because of the intense solar irradiation and reached values above 38 °C for most of the days with an overall maximum value of 55.8 °C on the 13th of August. For all these days the temperature indicates that a transition to the rutile state has occurred since hysteresis measurements in the lab indicate that above 38 °C at least 80% and at 47.6 °C the full transition from monoclinic to rutile is completed. Only 3 days could be observed in August where the maximum temperature in the smart window only reached between 29.2 and 33.4 °C, which indicates an

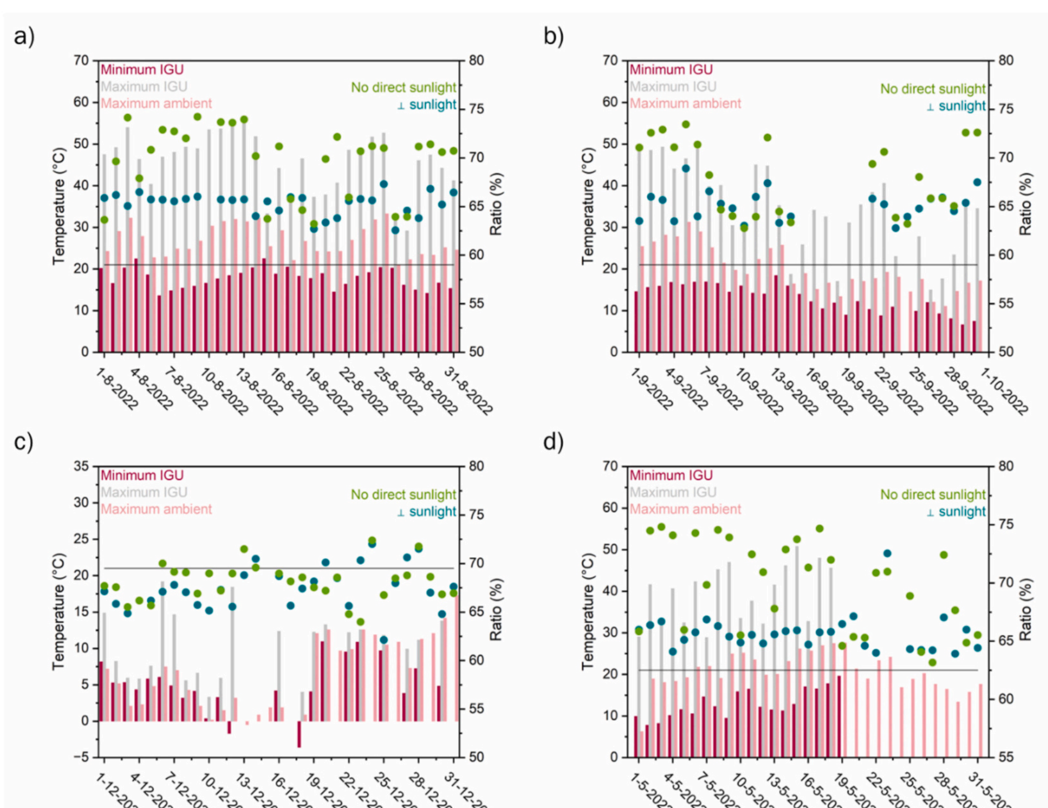


**Fig. 7.** Monthly overview of maximum (grey) and minimum (magenta) glass temperatures of the smart window, maximum ambient temperatures (pink), as well as transmission ratio at 12:00 (green) and 18:00 (turquoise) for representative months in a) summer, b) autumn, c) winter and d) spring. (For interpretation of the references to colour in this figure legend, the reader is referred to the web version of this article.)

incomplete transition of around 60%. The minimum temperature reached in the smart window during night was between 13.6 and 22.6 °C for all days in August. This suggests that only 20–50% of the functional material switched back from rutile to monoclinic on the individual days.

For the spectral measurements a clear difference between the 12:00 and 18:00 transmission ratio can be observed for most of the days. The 12:00 ratio is between 0.71 and 0.74 for most days and drops to between 0.64 and 0.66 during direct sunlight. Overall the spectral data correlate very well with the temperature data, showing a transition on each day from mainly monoclinic to rutile and back. Only on some days that start cloudy, the 12:00 ratio deviates, which can be explained by inaccuracies of the spectral measurement at low light intensities and passing clouds, as outlined in Section 3.3.1.1.

September, as the first autumn month, starts similar as August ended (Fig. 7b). Between the 1st and 13th of September 2022, maximum ambient temperatures between 18.8 and 31.3 °C were reached. Because of intense solar irradiance in the first half of September, the smart window temperature reached maximum values between 40 and 49 °C for all but 2 days in that time period. The minimum smart window temperature from 1 until 13. September was between 14.1 and 18.5 °C. As for August, these temperatures account for transition of more than 80% of all functional material to the rutile, IR blocking state during the day with a 20 to 50% switch back to monoclinic during night. The observed phase transition is again supported by the spectral data, where 12:00 ratios between 0.71 and 0.73 are observed, which drop to ratios between 0.63 and 0.66 during perpendicular sunlight. From 7th of September onwards days start to become more cloudy, which leads to transmission ratios deviating more significantly from the expected values and overall being more difficult to interpret.

For the second half of September maximum ambient temperatures start to drop consistently below 20 °C, reaching only between 11.1 and 19.3 °C between 14th – 30th of September. Maximum smart window temperatures fluctuate significantly between days, being severely influenced by clouding and rainfall. On mostly sunny days still maximum smart window temperatures between 35 and 41 °C are reached, representing between 70 and 86% of functional material transitioning to the rutile state. For mostly cloudy days the maximum smart window temperature is significantly lower and goes even down to 17.1 °C for individual days, representing only 10% of the functional material being transitioned to the rutile state. The minimum smart window temperature in the second half of September reaches values between 6.7 and 16 °C, representing up to 86% of functional materials transitioning back to the monoclinic phase overnight. The spectral data are difficult to interpret for the second half of September because of intense clouding resulting in measurement inaccuracies and errors due to inconsistent shading between smart window and reference IGU. Only 3 days with enough direct sunlight show the characteristic switch from a high transmission ratio around 0.72 in the morning to a low ratio around 0.66 in the afternoon, indicating a phase transition consistent with the temperature data.

In December as prototypical winter month, the ambient temperature stays below 12.5 °C for most of the days, with only the 30th and 31st of December reaching 14.2 and 17.3 °C, respectively (Fig. 7c). Especially in the first half of December, outdoor temperatures reach a maximum of only 0–2 °C. On these cold days also the smart window temperature stays relatively cool, even though direct solar radiation also here can lead to significant heat built up. The largest deviation of smart window temperature from ambient can be observed on December 12th, where the smart window reaches 18.5 °C, which is 15.3 °C above ambient and an increase of more than 450%. However, on most of the days the maximum window temperature stays below 12.5 °C. For these days the functional material stays to a large extent in the monoclinic phase with only up to 5% transitioning to rutile. Only on 2 days maximum smart window temperatures between 18.5 and 19.2 °C are reached where up to 14% of functional material undergoes a phase transition. Any material that transitions to rutile during the day in December transitions back to monoclinic in the night, where minimum smart window temperatures down to −3.6 °C are reached. The mostly static nature of the functional material is supported by the spectral data, which shows a relatively steady transmission ratio during individual days. Between days significant fluctuation in transmission ratio can be observed, which is caused by inaccuracies and errors due to cloud movement as described above.

In May, as a representative month in spring, the ambient temperatures start rising above 20 °C again (Fig. 7d). Between 1st and 8th of May, maximum ambient temperatures start rising from 18.1 to 22 °C. In the following days until 19th of May maximum ambient temperatures rise even up to 27.6 °C before they start to drop again towards the end of the month and reach between 13.4 and 17.7 °C. The period from 1st to 19th of May was characterized by high sunlight intensites and limited clouding, which led to maximum smart window temperatures reaching between 40.7 and 50 9 °C on mostly sunny days and between 28.9 and 37.7 °C for partially cloudy days. The smart window temperatures on sunny days represent a transition of between 85 and 97% of the functional material to the rutile state, whereas on partially cloudy days only between 48 and 80% underwent phase transition. Minimum smart window temperatures from 1st to 9th of May reach between 7.8 and 14.7 °C, which represents 45–85% of functional material switching back to monoclinic. From 10th to 19th of May the smart window stays between 11.3 and 19.7 °C, which means that only between 25 and 65% of functional material transitions back to the monoclinic crystal phase. Unfortunately, for the period from 20th to 31st of May the smart window temperatures were not recorded due to maintenance, which means that for these days the thermochromic switch can only be analyzed using the spectral data.

For the mostly sunny days between 1st and 19th of May, the spectral data show a very consistent trend for the transmission ratio. For most of the days the transmission ratio starts between 0.72 and 0.75 at the start of the day and then transitions to between 0.65 and 0.67 in the afternoon. This clear indication of a phase transition from monoclinic to rutile on each day confirms the interpretation of the temperature data for this part of the month. In the second part of the month, from May 20th – 31st, most days are characterized by heavy clouding, which complicates the analysis of the spectral data. Here for most days the transmission ratio cannot be analyzed due to inaccuracies and errors resulting from cloud movement. There are only three days, i.e. the 22nd, 25th and 28th, with enough sunlight to observe a clear transition from a high ratio between 0.69 and 0.72 to a low ratio between 0.64 and 0.67, indicating a thermochromic phase transition from monoclinic to rutile. For the remaining days, the crystal phase at individual times of the day cannot be analyzed.

### 3.3.3. *Seasonal overview*

Using the spectral and temperature analyses of the smart window IGU for individual days and months, an analysis of its performance within the 4 seasons can be executed. The meteorological seasons within the northern temperate zone were used for defining beginning and end of each season. For the seasonal performance, we investigated on which days a phase transition from monoclinic to rutile occurred and if this phase transition was desired based on a fixed performance criterium. As discussed in the previous chapters, the phase transition can either be detected by a change in optical properties or can be based on the measured glass temperature. In his chapter, a combination of both parameters will be used. For the interpretation if a phase transition is desired on an individual day, we use the measured ambient temperature. For optimized energy efficiency, the phase transition needs to be connected to a buildings thermostat. At ambient temperatures below the set temperature of a buildings thermostat, it can be assumed that solar heat is desired to contribute to heating up of the building, whereas at temperatures above this set point, it can be assumed that solar heat needs to be blocked to prevent overheating and unnecessary cooling demand. Therefore, in the most simple way, the thermostats set point can be used as ambient cut off temperature for the decision making of a desired and undesired switch. Here we selected 21 °C as the cut off, which means that days are defined as desired for a phase transition, when the maximum ambient temperature surpasses 21 °C, whereas when maximum ambient temperatures stay <21 °C they are defined as days where no phase transition is wanted. The selection of 21 °C as cut off temperature is based on average thermostat settings used in the Netherlands.

Investigating the summer months 2022, it can be observed that on most days a phase transition from monoclinic to rutile occurred within the smart window (Fig. 8a). In June the smart window stayed for only 28% of the days in the monoclinic state, which went further down to 13% in July and leading to 100% transition to the rutile state in the month of August. Looking at the maximum ambient temperatures reached between June and August 2022, it can be seen that on most of the days 21 °C was reached and surpassed (Fig. 8b). In June the maximum ambient temperature still stayed below 21 °C for 45% of the days. In July only 13% of the days did not reach 21 °C and in August all days surpassed the selected threshold temperature. Combing both sets of data, it can be concluded that in August and a large part of July, the smart window behaved as desired with phase transition to a solar IR bocking state on days that required a cooler indoor climate. In June there were a few days where the smart window already transitioned although the maximum ambient temperature stayed slightly below 21 °C. This indicates that the switching temperature of the doped $VO_2$ is slightly too low due to the significantly higher temperature of the glass pane in comparison to ambient at high solar irradiance levels. Furthermore, two days (one in June and one in July) can be observed where ambient temperatures >21 °C were reached, but a phase transition to the IR blocking state did not occur within the functional material. Looking into the detailed weather data on those days, it can be seen, that these days were dominated by intense clouds and very low irradiance levels <150 $W \cdot m^{-2}$. Therefore, the glass temperature stayed close to the ambient, only shortly reaching 21 °C and then dropping back below the phase transition temperature. Since on such days solar heat will not play a significant role in the heat up of a building, these results can be neglected for the performance evaluation of the smart window.

Investigating the gathered data for winter, collected from December 2022 until February 2023, the opposite picture can be observed (Fig. S7). Within the whole period the smart window stayed in the monoclinic, IR transparent state and the maximum ambient temperature stayed below 21 °C. Therefore, in winter an optimum performance for energy efficiency can be concluded with the smart window allowing solar heat to enter the building to contribute to space heating. Analyzing the data for spring and autumn results in a more complex behavior of the smart window in relation to the outside environment.

For autumn 2022, the first half of September continued the behavior observed in summer, where maximum ambient temperature exceeded 21 °C and the smart window transitioned to the rutile, IR blocking state (Fig. S8). In the second half of that month, ambient temperatures dropped below 21 °C, which led to the smart window staying in the IR transparent, monoclinic state. However, here also three days, the 21st, 22nd and 29th of September, can be observed where high solar irradiance led to glass temperatures of up to 40 °C, indicating a phase transition even though the ambient temperature stayed slightly below 21 °C. This behavior continues for October, where the maximum ambient temperature for individual days fluctuated between slightly above and slightly below 21 °C. Depending on the intensity of solar irradiance, the glass temperature either stayed close to ambient (at low irradiance) or reached temperatures that led to a phase transition (at high irradiance). Intense clouding in the period between 26th – 30th of October also led to days where the smart window stayed in the IR transparent state, even though maximum ambient temperatures exceeded 21 °C. Since for these days the state of the smart window is much more dependent on the irradiance than on the ambient temperature, only 57% of the days in October yield a desired behavior within the set evaluation criteria. November 2022 showed ambient temperatures dropping below 21 °C for the whole month. Here, as in the following winter, the smart window stayed for a large part in the IR transparent state, except for the 13th of November, where the high solar irradiance led to a glass temperature around 35 °C, indicating an undesired phase transition.

For spring, that is April–May 2022 and March 2023, a similar behavior of the smart window as in autumn can be observed (Fig. S9). Days with maximum ambient temperatures significantly below 21 °C or with low solar irradiance usually led to the smart window staying in the IR transparent state. Days with maximum ambient temperatures above 21 °C usually led to a phase transition to the IR blocking state. Whereas days with ambient temperatures slightly below 21 °C and high solar irradiances led to an unwanted transition to the IR blocking state of the smart window and days with ambient temperatures slightly above 21 °C and very low solar irradiances led to retention in the IR transparent state. In March ambient temperatures stayed below 21 °C for the whole month and the smart window kept optimum IR transparent properties. Between April 10th and May 13th, ambient temperatures fluctuated around 21 °C, leading to 14% of days in this time period, where phase transition occurred even though ambient temperatures stayed slightly below 21 °C. Starting from 7th of May also several days can be observed where ambient temperatures >21 °C were reached, but intense clouding prevented a phase transition to the IR blocking state.

### 3.3.4. Yearly overview

With the detailed analysis in previous chapters, an interpretation of the smart windows performance during the full year can be executed (Fig. 9). Giving the set evaluation criteria in Section 3.3.3., which are, that a phase transition is desired when maximum ambient temperatures of at least 21 °C are reached and that no phase transition is desired if the maximum ambient temperature stays <21 °C, it can be concluded that the smart window performs to a large extent within these requirements. Especially in winter, early spring and late autumn, when ambient temperatures are significantly below 21 °C, the window stays in the IR transparent state, allowing solar heat to contribute to space heating as much as possible. Furthermore, in the warmest period of the year, between July 2nd and September 20th, the smart window completely

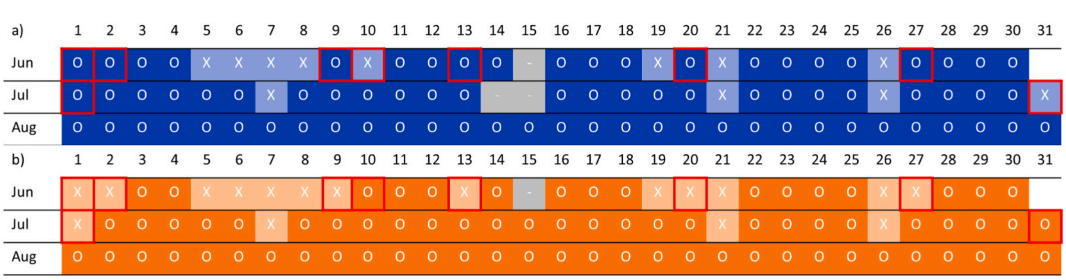


**Fig. 8.** Seasonal overview for summer 2022 on a) smart window transition state (X = IR transparent; O = IR blocking; – = missing data) and b) maximum ambient temperature reached (X ≤21 °C; O = ≥21 °C; – = missing data). Days on which smart window transition state and maximum ambient temperature reached do not match are marked in red. (For interpretation of the references to colour in this figure legend, the reader is referred to the web version of this article.)

| | 1 | 2 | 3 | 4 | 5 | 6 | 7 | 8 | 9 | 10 | 11 | 12 | 13 | 14 | 15 | 16 | 17 | 18 | 19 | 20 | 21 | 22 | 23 | 24 | 25 | 26 | 27 | 28 | 29 | 30 | 31 |
|---|---|---|---|---|---|---|---|---|---|---|---|---|---|---|---|---|---|---|---|---|---|---|---|---|---|---|---|---|---|---|---|
| Jan | O | O | O | O | O | O | O | O | O | O | O | - | O | O | O | O | - | O | O | O | O | O | O | O | O | O | O | O | O | O | O |
| Feb | O | O | O | O | O | O | O | O | O | O | O | O | O | O | O | - | - | O | O | O | O | O | O | O | O | O | - | - | | | |
| Mar | O | O | O | O | O | O | O | O | O | O | O | O | O | O | - | - | - | - | - | - | O | O | O | O | O | O | O | O | O | O | O |
| Apr | O | O | O | O | O | O | - | O | O | X | X | O | O | O | X | - | - | - | X | X | X | O | X | X | O | X | X | X | O | O | |
| May | O | X | X | X | O | O | x | X | O | x | O | O | X | O | O | x | O | O | O | x | O | O | x | - | O | O | O | O | O | O | O |
| Jun | X | X | O | O | O | O | O | O | X | x | O | O | X | O | - | O | O | O | O | X | O | O | O | O | O | O | X | O | O | O | |
| Jul | X | O | O | O | O | O | O | O | O | O | O | O | O | - | - | O | O | O | O | O | O | O | O | O | O | O | O | O | O | O | x |
| Aug | O | O | O | O | O | O | O | O | O | O | O | O | O | O | O | O | O | O | O | O | O | O | O | O | O | O | O | O | O | O | O |
| Sep | O | O | O | O | O | O | O | O | O | O | O | O | O | O | O | O | O | O | O | O | X | X | O | O | O | O | O | O | X | O | |
| Oct | O | O | O | X | O | X | X | X | X | O | X | - | O | O | O | O | O | X | O | O | X | O | O | O | O | x | x | x | x | x | O |
| Nov | O | O | O | O | O | O | O | O | O | O | O | O | X | O | O | O | O | O | O | O | O | O | O | O | O | O | O | O | O | O | |
| Dec | O | O | O | O | O | O | O | O | O | O | O | O | O | O | - | O | O | O | O | O | O | O | O | O | O | O | O | O | O | O | O |

**Fig. 9.** Full year analysis of smart window performance (O = desired behavior; X = undesired transition; x = undesired retention; − = missing data).

transitioned to the IR blocking state, contributing to a cool indoor climate. Only in the periods between April 10 – July 1 and between September 21 – October 31, significant deviation from desired performance can be observed. In these periods, which represent a transition from cold to warm temperatures and vice versa, maximum ambient temperatures fluctuate around 21 °C and several days can be observed, where the smart window transitions too early. This means that on days, where contribution of solar heat to space heating is still desired, the smart window already transitions to the IR blocking state. This effect can be attributed to the significantly higher glass temperature in comparison to ambient at high irradiance levels. The heat accumulation in the glass, which is affected by light absorption of the functional material and the glass itself, leads to a phase transition of the functional $VO_2$. Since the transition temperature of the $VO_2$ particles was designed with the ambient temperature as reference, it can be concluded that to optimize performance, it has to be slightly increased, using the obtained glass temperatures and not the ambient temperature as reference. Furthermore, a number of days can be observed where intense clouding leads to retention of the smart window in the IR transparent state, even though maximum ambient temperatures >21 °C are reached. However, since on these days solar heat will not play a significant role in the heat up of a building, these results can be neglected for the performance evaluation of the smart window. Looking at the glass temperatures for all days between April and November, where an undesired phase transition occurred, it can be concluded that a $T_{switch}$ between 35 and 40 °C would be most beneficial for the here investigated scenario. However, this suggestion needs to be confirmed to not induce negative effects via undesired retentions on other days and it has to be mentioned that other IGU configurations (e.g. different glass thicknesses, using thermochromic coatings instead of laminated glass, or using triple instead of double glazing) as well as other geographical regions can lead to differences in requirements for optimized $T_{switch}$. Finally, the most optimum performance will always be a balance between reducing undesired transitions as much as possible whilst keeping undesired retentions to a minimum.

## 4. Conclusion and outlook

In conclusion, we have executed an in depth, full year study on the performance and functionality of a $VO_2$-based thermochromic smart window under real-life conditions. For the first time, we have monitored light and solar transmission connected with glass and ambient temperatures, which enabled us to investigate the thermochromic phase transition and adaptive solar heat gain of a thermochromic interlayer (laminate) in real-life environment. Studying the performance and functionality of the smart window per day, month, season and year led to the following significant conclusions:

- Temperature and magnitude of the thermochromic switch in real life are very comparable to lab measurements.
- With direct sunlight on the smart window and glass temperatures exceeding the phase transition temperature of the implemented $VO_2$, the thermochromic interlayer transitions to an IR blocking state.
- At direct sunlight, glass surface temperatures of reference glass and thermochromic glass are significantly higher than ambient temperature, with an increase of up to 50% or 100%, respectively, in comparison to the respective ambient temperature.
- On sunny days, the thermochromic phase transition can be monitored very well and the smart windows functionality is matching the desired properties with transition to the blocking state at high ambient temperatures and retention in the transparent state at low temperatures.
- On cloudy days, low light intensities, inhomogeneous clouding and reflection patterns lead to inconclusive results from the spectral measurements. Here only temperature data can be used to interpret the phase transition. For most cloudy days the smart window stays in the transparent state with only days with very high ambient temperatures leading to a phase transition.
- Partially sunny and cloudy days can be depicted as combinations of behavior observed for both full sunny and full cloudy days. These have to be analyzed on an individual basis.
- Smart window performance in summer and winter is mostly according to expectations with phase transition to IR blocking state on warm days and retention in IR transparent state on cold days.
- In spring and autumn days, where the ambient temperature stays close to 21 °C, undesired behavior in the smart window can occur. Here, high solar intensities can lead to an undesired phase transition at ambient temperatures <21 °C and intense clouding can lead to undesired retention in the transparent state at ambient temperatures >21 °C.
- Undesired phase retention only occurs on days with very low light intensities. Because of the minimal overall impact of sunlight on space heating on these days, the undesired behavior can be ignored.
- Undesired phase transition is caused by light absorption of the glass and photothermal heating of the thermochromic interlayer. The smart window then shows a significantly higher glass surface temperature than respective ambient temperature. This effect leads to reduced contribution of sunlight to space heating under cold conditions and therefore needs to be counteracted for optimized energy efficiency of the smart window.
- To reduce the number of days with undesired phase transition, a $T_{switch}$ around 35–40 °C is suggested for the here studied scenario.

Overall it can be concluded, that the smart window largely performs according to the expected and desired requirements for optimized energy efficiency. However, the selected switching temperature was slightly too low, since it was designed with the ambient temperature in mind not taking photothermal heating into account. The study has shown that the switching temperature has to be instead designed towards the measured glass surface temperatures to further improve energy efficiency and prevent premature phase transition.

For next steps, the thermochromic material needs to be modified for a $T_{switch}$ around 35–40 °C via reduced amount of W doping. With an optimized smart window more advanced real-life studies can be executed monitoring heating and cooling loads and investigating the impact of the smart window on occupants health and comfort.

## Supporting information

Laser diffraction measurements of W-doped $VO_2$ particles (Fig. S1); Placement of FBG sensors (Fig. S2); FBG calibration (Fig. S3); Time dependent transmission spectra at 500 nm (Fig. S4); temperature measurements of individual FBG sensor gratings (Fig. S5); photothermal heating experiments (Fig. S6); seasonal overview for winter, autumn and spring (Fig. S7-S9).

## CRediT authorship contribution statement

**Romy van Geijn:** Visualization, Investigation, Formal analysis. **Ryan van Zandvoort:** Investigation, Formal analysis. **Luc Leufkens:** Validation, Formal analysis. **Janique Hupperetz:** Validation, Investigation. **David Out:** Methodology, Investigation, Formal analysis. **Rémi Aninat:** Methodology, Investigation, Formal analysis. **Roland Valckenborg:** Validation, Supervision, Conceptualization. **Nicole Meulendijks:** Supervision, Project administration, Funding acquisition. **Phillippe Nivelle:** Methodology, Investigation, Formal analysis. **Michaël Daenen:** Validation, Supervision, Conceptualization. **Daniel Mann:** Writing – review & editing, Writing – original draft, Visualization, Supervision, Methodology, Conceptualization. **Pascal Buskens:** Writing – review & editing, Supervision, Conceptualization.

## Declaration of competing interest

The authors declare the following financial interests/personal relationships which may be considered as potential competing interests: Romy van Geijn, Ryan van Zandvoort, Luc Leufkens, Janique Hupperetz, David Out, Remi Aninat, Roland Valckenborg, Nicole Meulendijks, Phillippe Nivelle, Michael Daenen, Daniel Mann and Pascal Buskens reports financial support was provided by Interreg V program Flanders-The Netherlands. Phillippe Nivelle, Michael Daenen reports financial support was provided by Belgian province of Limburg. Romy van Geijn, Ryan van Zandvoort, Luc Leufkens, Janique Hupperetz, Nicole Meulendijks, Daniel Mann and Pascal Buskens reports was provided by Dutch province of Limburg. David Out, Remi Aninat, Roland Valckenborg reports was provided by Dutch province of Noord-Brabant. If there are other authors, they declare that they have no known competing financial interests or personal relationships that could have appeared to influence the work reported in this paper.

## Acknowledgment

The authors acknowledge financial support from the European Fund for Regional Development through the cross-border collaborative Interreg V program Flanders-The Netherlands (project SUNOVATE), co-financed by the Belgian province of Limburg and the Dutch provinces of Limburg and Noord-Brabant.

## Appendix A. Supplementary data

Supplementary data to this article can be found online at https://doi.org/10.1016/j.enbuild.2026.117881.

## Data availability

Data will be made available on request.

## References

[1] L. Aditya, T.M.I. Mahlia, B. Rismanchi, H.M. Ng, M.H. Hasan, H.S.C. Metselaar, O. Muraza, H.B. Aditiya, A review on insulation materials for energy conservation in buildings, Renew. Sust. Energ. Rev. 73 (2017) 1352–1365.

[2] K. Tsikaloudaki, T. Theodosiou, K. Laskos, D. Bikas, Assessing cooling energy performance of windows for residential buildings in the Mediterranean zone, Energy Convers. Manag. 64 (2012) 335–343.

[3] S. Jaber, S. Ajib, Thermal and economic windows design for different climate zones, Energ. Buildings 43 (2011) 3208–3215.

[4] Y. Ke, J. Chen, G. Lin, S. Wang, Y. Zhou, J. Yin, P.S. Lee, Y. Long, Smart windows: electro-, thermo-, mechano-, photochromics, and beyond, Adv. Energy Mater. 9 (2019) 1902066.

[5] Z. Zhang, L. Zhang, Y. Zhou, Y. Cui, Z. Chen, Y. Liu, J. Li, Y. Long, Y. Gao, Thermochromic energy efficient windows: fundamentals, recent advances, and perspectives, Chem. Rev. 123 (2023) 7025–7080.

[6] Y. Cui, Y. Ke, C. Liu, Z. Chen, N. Wang, L. Zhang, Y. Zhou, S. Wang, Y. Gao, Y. Long, Thermochromic $VO_2$ for energy-efficient smart windows, Joule 2 (2018) 1707–1746.

[7] L. Calvi, L. Leufkens, C.P.K. Yeung, R. Habets, D. Mann, K. Elen, A. Hardy, M. K. Van Bael, P. Buskens, A comparative study on the switching kinetics of W/$VO_2$ powders and $VO_2$ coatings and their implications for thermochromic glazing, Sol. Energy Mater. Sol. Cells 224 (2021) 110977.

[8] L. Calvi, R. van Geijn, L. Leufkens, R. Habets, K.L. Gurunatha, K. Stout, D. Mann, I. Papakonstantinou, I.P. Parkin, K. Elen, A. Hardy, M.K. van Bael, P. Buskens, The impact of bead milling on the thermodynamics and kinetics of the structural phase transition of $VO_2$ particulate materials and their potential for use in thermochromic glazing, Sol. Energy Mater. Sol. Cells 242 (2022) 111783.

[9] K. Timmers, A. Chote, L. Leufkens, R. Habets, K. Elen, M.A. Verheijen, A.K. Van Bael, D. Mann, P. Buskens, Hydrothermal synthesis of monoclinic $VO_2$ microparticles without use of hazardous reagents: a key role for the W-dopant, Inorg. Chem. 63 (2024) 5400–5413.

[10] C.P.K. Yeung, R. Habets, L. Leufkens, F. Colberts, Z. Vroon, D. Mann, P. Buskens, Phase separation of $VO_2$ and $SiO_2$ on $SiO_2$-coated float glass yields robust thermochromic coating with unrivalled optical properties, Sol. Energy Mater. Sol. Cells 230 (2021) 111256.

[11] L. Calvi, R. van Zandvoort, L. Leufkens, J.F.B. Hupperetz, R. Habets, D. Mann, N. Meulendijks, K. Elen, M.A. Verheijen, A. Hardy, M.K. Van Bael, P. Buskens, Thermochromic glass laminates comprising W/$VO_2$ nanoparticles obtained by wet bead milling: an in-depth study of the switching performance, Sol. Energy Mater. Sol. Cells 257 (2023) 112350.

[12] Z. Shao, X. Cao, H. Luo, P. Jin, Recent progress in the phase-transition mechanism and modulation of vanadium dioxide materials, NPG Asia Mater. 10 (2018) 581–605.

[13] J. Zhu, Y. Zhou, B. Wang, J. Zheng, S. Ji, H. Yao, H. Luo, P. Jin, Vanadium dioxide nanoparticle-based thermochromic smart coating: high luminous transmittance, excellent solar regulation efficiency and near room temperature phase transition, ACS Appl. Mater. Interfaces 7 (2015) 27796–27803.

[14] J. Schläfer, C. Sol, T. Li, D. Malarde, M. Portnoi, T.J. Macdonald, S.K. Laney, M. J. Powell, I. Top, I.P. Parkin, I. Papakonstantinou, Thermochromic $VO_2$ - $SiO_2$ nanocomposite smart window coatings with narrow phase transition hysteresis and transition gradient width, Sol. Energy Mater. Sol. Cells 200 (2019) 109944.

[15] D. Mann, C.P.K. Yeung, R. Habets, R. Van Zandvoort, L. Leufkens, J. Hupperetz, D. Out, R. Valckenborg, Z. Vroon, P. Buskens, SunSmart – the first affordable, energy optimized smart window, IOP Conf. Ser. Earth Environ. Sci. 1085 (2022) 012060.

[16] D. Mann, L. Calvi, C.P.K. Yeung, R. Habets, K. Elen, A. Hardy, M.K. Van Bael, B. Buskens, Approaching the theoretical maximum performance of highly transparent thermochromic windows, Energies 16 (2023) 4984.

[17] D. Mann, C. Yeung, R. Habets, Z. Vroon, P. Buskens, Comparative building energy simulation study of static and Thermochromically adaptive energy-efficient glazing in various climate regions, Energies 13 (2020) 2842.

[18] D. Mann, C.P.K. Yeung, R. Habets, Z. Vroon, P. Buskens, Building energy simulations for different building types equipped with a high performance thermochromic smart window, IOP Conf. Ser. Earth Environ. Sci. 855 (2021) 012001.

[19] M.E.A. Warwick, I. Ridley, R. Binions, The effect of variation in the transition hysteresis width and gradient in thermochromic glazing systems, Sol. Energy Mater. Sol. Cells 140 (2015) 253–265.

[20] R. Tällberg, B.P. Jelle, R. Loonen, T. Gao, M. Hamdy, Comparison of the energy saving potential of adaptive and controllable smart windows: a state-of-the-art review and simulation studies of thermochromic, photochromic and electrochromic technologies, Sol. Energy Mater. Sol. Cells 200 (2019) 109828.

[21] H. Kim, Y. Kim, K.S. Kim, H.Y. Jeong, A.-R. Jang, S.H. Han, D.H. Yoon, K.S. Suh, H. S. Shin, T.Y. Kim, W.S. Yang, Flexible thermochromic window based on hybridized $VO_2$/graphene, ACS Nano 7 (2013) 5769–5776.

[22] Y. Gao, H. Luo, Z. Zhang, L. Kang, Z. Chen, J. Du, M. Kanehira, C. Cao, Nanoceramic $VO_2$ thermochromic smart glass: a review on progress in solution processing, Nano Energy 1 (2012) 221–246.

[23] T. Chang, X. Cao, L.R. Dedon, S. Long, A. Huang, Z. Shao, N. Li, H. Luo, P. Jin, Optical design and stability study for ultrahigh-performance and long-lived vanadium dioxide-based thermochromic coatings, Nano Energy 44 (2018) 256–264.
[24] H. Ye, L. Long, H. Zhang, B. Xu, Y. Gao, L. Kang, Z. Chen, The demonstration and simulation of the application performance of the vanadium dioxide single glazing, Sol. Energy Mater. Sol. Cells 117 (2013) 168–173.
[25] R.C.G.M. Loonen, M.L. de Klijn-Chevalerias, J.L.M. Hensen, Opportunities and pitfalls of using building performance simulation in explorative R&D contexts, J. Build. Perform. Simul. 12 (2019) 272–288.
[26] P. Nivelle, L. Maes, J. Poortmans, M. Daenen, In situ quantification of temperature and strain within photovoltaic modules through optical sensing, Prog. Photovolt. Res. Appl. 31 (2023) 173–179.